Aerosol radiative forcing during African desert dust events (2005-2010) over south-eastern Spain.

By **A.Valenzuela[1,2], F.J. Olmo[1,2], H. Lyamani[1,2], M. Antón[1, 2], A. Quirantes[1]**

and L. Alados-Arboledas[1,2]

Atmospheric Chemistry and Physics

avalenzuela@ugr.es

Answers to Editor Comments:

The authors greatly acknowledge the Editor for carefully reading the manuscript and providing constructive comments. Following the suggestions we will make changes in the manuscript and here in bold responses to Editor Comments.

1. Presentation of the forcing calculation results. The description of aerosol forcing should be clearly described. The authors should clarify if they calculated instantaneous values or daily averages, how calculations were done (which properties of aerosol and surface reflectance were used, how their spectral variability was accounted). If the authors noted some important tendencies in the forcing variability it would be useful to discuss the causes of this variability. For example, if it is caused by variability in aerosol SSA, it could be useful to display and discuss values of SSA.

The aerosol radiative forcing have been simulated using as input in the SBDART radiative transfer model the experimental aerosol information (aerosol optical depth, single scattering albedo and asymmetry parameter) derived from the principal plane retrievals. Logarithmic interpolation (or extrapolation for $\lambda < 414$ nm or $\lambda > 860$ nm) was used to supply SBDART with aerosol optical depths covering the entire wavelength range of the calculation (310–2800 nm). Linear extrapolation is used for single scattering albedo and asymmetry parameter. In the new version of the manuscript, we have re-calculated all simulated values of the aerosol radiative forcing, taking into account the spectral dependence of the surface albedo at the study site. For that, we used as input in the SBDART code the surface spectral albedo information provided by the AERONET network at Granada station, which is based on a dynamic spectral and spatial model estimation at four wavelengths: 440, 675, 870 and 1020 nm. This algorithm adopted the Lie-Ross model for land surface covers (Lucht and Roujean, 2000), considering the bidirectional reflectance distributions taken from MODIS (Moody et al., 2005).

The average values of the aerosol radiative forcing given in the old version of the manuscript were calculated from instantaneous values. However, according to the referees suggestions we have computed the daily mean aerosol radiative forcing at surface and TOA (24 hour averages) as in (Bush and Valero, 2003):

$$DARF = \int \frac{ARF dt}{24}$$

In addition we have computed the atmospheric heating rate following Liou (2002) as:

$$\frac{\Delta T}{\Delta t} = \frac{g}{C_p}\frac{\Delta F}{\Delta p}$$

where T is the temperature (K), t is the time (s), g is the gravitational acceleration (ms^{-2}), C_p is the specific heat of dray air (JK^{-1}), F is the net all-wave flux (Wm^{-2}), and p is the pressure (Pa).

The results of these new computations have been included and discussed in the new version of the manuscript.

In order to justify and discuss the aerosol radiative forcing results, we have added in the new version of the manuscript more information about aerosol optical properties (aerosol optical depth and single scattering albedo). In fact, we have incorporated a new table with aerosol optical and microphysical properties.

2. Generation of aerosol properties. One of the declared novelties of presented studies is the fact that authors used the aerosol properties derived from principle plane observation. However, the authors do not provide any description of their approach for assuring quality of their retrievals. For example, the standard AERONET products are filtered out by numerous cloud-screening and quality assurance criteria (e.g. see Dubovik et al. 2002). In these regards, the advantage of the observations in the almucantar is a possibility to filter out the partially cloudy data by checking symmetry of left and right almucantars scans. Such check is not possible for principle plane and therefore screening partially cloudy data is more challenging. In any case the authors should carefully describe the used procedure for quality assurance of the data. Also, I am aware that some radiances given by AERONET website for principle plane data are lower quality than the radiances for almucantar. I suggest that the authors contact the AERONET staff and verify that issue.

Thanks for these comments. In the next section (3) we will provide more information about the methodology and quality assurance procedures.

Regarding the calibration factors of the CIMEL-CE318 sun-photometer used in this work (spectral extinction and sky radiances), these were performed by AERONET/RIMA facilities at Valladolid (Spain) following the standardized network procedures (instrument maintenance and calibration). The calibration period is approximately 1 year. This instrument is part of the AERONET network from 2004. The assumed calibration errors are lower than 5%. In the new version of the manuscript we used the data-base (aerosol optical parameters) provided by AERONET web page (Level 2.0) and also the data-base derived by our methodology using the same raw data (K7 files) and the calibration factors performed by the AERONET/RIMA facilities.

Other error sources in sky radiance measurements are the error during the pointing process (misalignments) due to the motors motion (azimuth and zenith axes) used by CIMEL instruments, and the error associated with the considered value of the field of view. Torres (2012) analyzes the pointing error (vertical and

horizontal errors) in terms of the scattering angle, showing that the bias introduced during the measurements in a middle latitude station can be estimated in the range 0-0.4°. This error source affects more the principal plane measurements (especially the vertical error) than the almucantar measurements, changing the observed radiance values as a function of the scattering angle, and it can be an explanation for discrepancies in the derived products observed by the AERONET network. These anomalies will take place for largest errors and shortest scattering angles, when radiance function varies more rapidly, showing lower $SSA(\lambda)$ values at noon (about 10% or more) while the $AOD(\lambda)$ values present no significant variability. On the other hand, the evaluation of the error in the field of view (instrumental limitation) on the radiance measurements showed a negligible influence on the retrieved aerosol products (e.g. Torres, 2012). From our results using the principal plane inversion methodology (see the next paragraph (3)), these discrepancies were not detected in the derived aerosol products, although they could be masked with the other instrumental errors.

Furthermore, several issues related to the error sources and the inversion products (almucantar and principal plane) are currently investigated within the AERONET community. In fact, almucantar and principal plane retrievals present differences that may be attributed to measurement errors and/or model inaccuracies (e.g. Torres, 2012).

Regarding the clouds filter, as the Editor states, one of the major difficulties of the sky radiance retrievals in principal plane and almucantar configurations is the cloud screening procedure. For the almucantar configuration, it is possible to use the symmetry analysis of the left and right parts of the sky radiance measurements. For the principal plane this quality control is more difficult and possibly the sky radiance measurements may have more errors than for almucantar configuration. However, the symmetry criteria cannot be applied on the principal plane data. In this study, to eliminate cloud contaminated aerosol optical depths, and the corresponding principal plane sky radiance measurements, first we applied the triplet stability criteria (Smirnov et al., 2000) to the spectral extinction data measured at the beginning of the principal plane scan. Even if data pass the threshold screening test, we only take data within three standard deviations from the mean in order to further reduce uncertainties induced by cloud contamination. In fact, high differences between two consecutive values of $AOD(\lambda)$ data are usually associated with passing clouds or aerosol in-homogeneities. In addition, the possible influence of thin clouds and spatially inhomogeneous clouds, which are difficult to completely eliminate and could contribute to the sky radiance errors, have been considered. Thus, we have obtained a smoothed principal plane sky radiance data set by applying a moving average smoothing algorithm with slide window of five-point width. If the maximum difference between the smoothed and the initial sky radiances set (point to point) was higher than threshold 5% the data were rejected. Also, if the number of scattering angles in the measured sky radiance distributions is less than 20, the measurements record is eliminated. In addition, in order to accept a principal plane inversion as valid the relative differences (residuals) between the measured and computed normalized sky radiances must be less than 10%. Finally, to eliminate those clouds contaminated sky radiances that passed the previous filters we used a supervised inspection of sky images acquired with an All-Sky Imager

(e.g. Cazorla et al., 2008). Therefore, we would like to highlight that the procedure is based on a combination of automatic procedures and human supervised analyses of ancillary information in order to guarantee the quality of the principal plane retrieval.

According to our experience this cloud screening procedure assures the data quality. For instance, Figure 1(a, b) shows the all-sky images registered for two consecutive days at the same hour (October 6, 2010, 10:15 h GMT –cloudless- and October 7, 2010, 10:15 h –clouds-). Also, Figure 1c shows the evolution of the normalized principal plane sky radiances derived for the two situations. It can be seen that there are differences directly attributed to the presence of clouds at large scattering angles. These variations in normalized sky radiances cause the rejection of this case (October 7, 2010, 10:15 h) with the applied triplet stability criteria and the threshold of 5% between the smoothed and the initial sky radiances.

3. The details of the retrieval scheme/algorithm used by the authors should be well described. The text of the paper suggests that the authors used rather original approach. However, the originality and efficiency of the approach remain unclear. It seems that the authors used SKYRAD package (by Nakajima et al.) updated with spheroid-based model. Is this correct? Are there any other modification for SKYRAD? How different the new spheroid model from the one used by AERONET. Are there any advantages of disadvantages? The authors stated that they used T-matrix calculation, but how they managed to make calculations for the particles with large size parameter, where T-matrix calculations do not converge? What is the range of axis ratios in generated kernels, etc.? How does the complex refractive index and SSA are retrieved? (cited paper of Nakajima et al. 1996 does not describe this). Some illustrations of aerosol retrievals also would be useful for understanding if there were any differences with AERONET products and if they can cause any differences in calculated values of forcing.

With regards to the methodology used we would like to thank for comments and suggestions that have led us to consider the inclusion of additional details in this particular aspect.

The method used in this study is based on the original method developed by Nakajima et al. (1996), SKYRAD.PACK, that gives the option to invert the almucantar or the principal plane sky radiance measurements. This method, and successive improvements, was applied by SKYNET network to retrieve aerosol properties from Prede POM radiometer measurements and was also implemented by AERONET network in a first stage for CIMEL CE-318 sun-photometer measurement retrievals. This method is based on spherical particles assumption. However, most of atmospheric particles have non spherical shapes (e.g. desert dust) and thus it is necessary to account for particle shape non-sphericity in order to obtain more accurate aerosol properties retrievals.

In this sense, we have updated the SKYRAD.PACK software with spheroid-based model to account for particle non-sphericity in the modelling of aerosol properties, and also implementing an iterative procedure to derive the refractive index and

the other aerosol optical parameters. As input parameters we used the spectral normalized sky radiances in the principal plane configuration, the spectral aerosol optical depth values measured at the beginning of the principal plane scan (as fixed values for the iterative process) and several constant values associated with the convergence criteria. If we use only spectral values of normalized sky radiance as input data, and taking into account the different error sources associated with the measurements, our experience shows that the inversion model could not accurately retrieve the spectral dependence of the aerosol optical depth and single scattering albedo.

The non-spherical kernels matrices used (look-up tables) are computed by the T-matrix method assuming randomly oriented prolate and oblate spheroids, using equiprobable distributions, following the recommendations of Dubovik et al. (2002a, 2006). By iteration, the algorithm retrieves first the real part of the refractive index -assuming the imaginary part as zero- and then, fixing the real part, the imaginary part is retrieved. The refractive indices used are assumed invariant with wavelength, and are varied in the ranges 1.33–1.60 (0.02 step) and 0–0.01 (0.0005 step) for the real part and imaginary part, respectively. The procedure search for the solution minimizing the residuals between measured and simulated normalized sky radiances (<10%), and also minimizing the RMSE –root mean square error- between the measured and simulated aerosol optical depth values (RMSE<5%). As output parameters we acquired the refractive index, the effective aerosol volume size distribution, the single scattering albedo, the phase function and the asymmetry parameter.

In the following paragraphs we show a brief of the SKYRAD.PACK modifications, including more details and also the limitations and differences with the well tested AERONET algorithm. Finally, we also analyse the accuracy assessment for individual retrievals.

First, we use as input in code the spectral aerosol optical depth values (as fixed parameters) derived by the Beer's law. In this sense, the monochromatic direct solar irradiance, F (Wm^{-2}μm^{-1}), is given by:

$$F_\lambda = F_{o\lambda} \exp(-m_o \tau_\lambda) \qquad\qquad (1)$$

where F_o is the monochromatic irradiance at the upper limit of the atmosphere; m_o is the optical air mass; and τ, the total atmospheric optical depth. If the extraterrestrial irradiance, F_o, is known (related to the instrument calibration factor) and the ground irradiance, F, is measured, then the aerosol optical depth under cloud-free conditions, τ_a, can be retrieved from this equation after subtraction of the Rayleigh scattering, corrected by local pressure, and gas absorptions (O_3 and NO_2) optical depth. In this study, the spectral aerosol optical depth is derived from the total optical depth obtained from direct sun photometer measurements data using the appropriate calibration constants provided by AERONET (linear rate change in time is assumed for calibration constants) and subtracting the Rayleigh optical depth, as well as the optical depths for O_3 and NO_2 following the methodology described by (Alados et al., 2003, 2008). The total

estimated uncertainty in aerosol optical depth is of ±0.01 for λ>400 nm and ±0.02 for shorter wavelengths (Alados et al., 2003). In our procedure the information about the wavelength dependence of $\tau_a(\lambda)$ is known.

For more accurate aerosol properties retrievals, the SKYRAD.PACK code uses as input the monochromatic sky radiance normalized by the monochromatic direct solar irradiance, $R(\Theta, \lambda)$, instead of the monochromatic sky radiance, that is a magnitude less affected by interference filters degradation of sun-photometers, and can be more accurately determined. In our case:

$$R(\Theta, \lambda) = \frac{E(\Theta, \lambda)}{F_\lambda m_o \Delta\Omega} \qquad (2)$$

where $E(\Theta,\lambda)$ is the monochromatic sky radiance measured, F_λ is the monochromatic direct solar irradiance from equation (1), and $\Delta\Omega$ is the solid view angle of the sky radiometer. The AERONET algorithm also uses the normalized sky radiances as input parameter, but normalized by the monochromatic extraterrestrial direct solar irradiance. On the other hand, the normalized sky radiance can be accurately determined in inversion code by:

$$R(\Theta, \lambda) = \beta(\Theta, \lambda) + q(\Theta, \lambda) \qquad (3)$$

where $\beta(\Theta,\lambda)$ is the total differential scattering coefficient (single scattering term), that is the sum of the scattering coefficients for aerosol and molecules, and $q(\Theta,\lambda)$ is the multiple-scattering term. The contribution of the multiple-scattering term can be significant. For example, at Θ=60º and λ=0.5 μm this contribution is of 41% when solar zenith angle is close to 30º and τ_a=0.2. Thus, an accurate scheme for the multiple-scattering treatment is needed. In this sense, SKYRAD.PACK code includes an accurate radiative transfer modelling in order to account for multiple scattering effects.

In solutions approach of equation (3), the atmospheric layers are characterized by its optical depth, single scattering albedo and phase function, and the scattering properties of an atmospheric aerosol layer are modelled by averaging single-particle properties. To derive the solutions the SKYRAD.PACK code uses the spherical approximation for single-particle properties. In our case, the aerosol single-scattering term, $\beta(\Theta)$, can be defined as functions of the volume size distribution of randomly oriented, polydisperse spheroids (e.g. Dubovik et al., 2006):

$$\beta(\Theta, \lambda) = \int_{\ln \varepsilon_{min}}^{\ln \varepsilon_{max}} \int_{\ln r_{min}}^{\ln r_{max}} \frac{C_{scat}(\lambda, \Theta, n, k, \varepsilon, r)}{v(r)} \frac{dn(\varepsilon)}{d\ln(\varepsilon)} \frac{dV(r)}{d\ln r} d\ln r\, d\ln\varepsilon \qquad (4)$$

$$\tau_{ext}(\lambda) = \int\limits_{\ln \varepsilon_{\min}}^{\ln \varepsilon_{\max}} \int\limits_{\ln r_{\min}}^{\ln r_{\max}} \frac{C_{ext}(\lambda,n,k,\varepsilon,r)}{v(r)} \frac{dn(\varepsilon)}{d\ln(\varepsilon)} \frac{dV(r)}{d\ln r} d\ln r\, d\ln \varepsilon \qquad (5)$$

where ε is the axis ratio of the spheroid and r the radius of a volume-equivalent sphere (same volume as the spheroid); τ_{scat} and τ_{ext} are the scattering and extinction optical depth; C_{scat} and C_{ext} are the scattering and extinction cross sections; n is the real part of the refractive index; k is the imaginary part of the refractive index; $v(r)$ is the volume of the particle with radius r; $dV/dlnr$ is the volume size distribution; and $dn(\varepsilon)/dln\varepsilon$ is the distribution of the spheroid axis ratios.

Following the recommendations of Dubovik et al. (2002, 2006), pre-computed look-up tables of aerosol scattering and extinction properties were used to reduce the computation time. The integration of equations (4) and (5) can be approximated by using the kernels K_{ext} and K_{scat}:

$$\beta(\Theta,\lambda) \approx \sum_{p,k} \frac{dn(\varepsilon_p)}{d\ln \varepsilon} \frac{dV(r_k)}{d\ln r} K_{scat}(\Theta,\lambda,n,k,\varepsilon_p,r_k) \qquad (6)$$

$$\tau_{ext}(\lambda) \approx \sum_{p,k} \frac{dn(\varepsilon_p)}{d\ln \varepsilon} \frac{dV(r_k)}{d\ln r} K_{ext}(\lambda,n,k,\varepsilon_p,r_k) \qquad (7)$$

where $dn(\varepsilon_p)/dln\varepsilon$ and $dV(r_k)/dlnr$ are the values of the size distributions $dn(\varepsilon)/dln\varepsilon$ and $dV(r)/dlnr$ given at discrete logarithmically equidistant points. The kernels can be pre-computed, and their dependence on n and k can be parameterized by a look-up table covering the range of expected values. In this paper the EBCM, or T-matrix (Waterman, 1971), theory has been used to calculate light scattering for non-spherical matrices (kernel matrices). Convergence procedures have been set so that phase matrix elements are calculated with accuracy of 10^{-3}; cross sections are accurate to within one part in 10^4 (Mishchenko, 1993). The kernel matrices are computed for 74 scattering angles, from 0 to 180º, using randomly oriented prolate and oblate spheroids (equiprobable distributions). Numerical test and inversion of the measurements showed an improvement of the retrieval stability using the assumption of an equal presence of prolate and oblate spheroids (Dubovik et al. 2002a, 2006).

The specific size limits for stable performance of the T-matrix code depend of ε. In addition, the size limit can be different for the same ε with different n and k. The T-matrix code becomes numerically unstable for spheroids with $\varepsilon \sim 2$-2.4 and size parameters x ($=2\pi r/\lambda$) larger than about 60. Actually, using the T-matrix method, our kernel matrices computations are limited to the following range of aerosol parameters:

$1.33 \le n \le 1.6$

$0.0005 \leq k \leq 0.64$

$0.6 \leq \varepsilon \leq 3.0$

$0.01 \leq x \ (=2\pi r/\lambda) \leq 148.9$

and the integration has been performed for the different aspect ratios and for N_x x N_n x N_k sample points in a logarithmic scale. For the values of n and k between the sampling points, K_{ext} and K_{scat} were linearly interpolated on the logarithmic scale. The range of aerosol parameters is a serious limitation of the look-up tables used in this work. The results show that it is necessary to consider aerosol particles with sizes up to at least $x \sim 100\text{-}120$ in order to account for ~99% of the scattering signal (e.g. Dubovik et al., 2002). Future improvements using other methods such as the geometric-optics-integral-equation method (e.g. Yang and Liou, 1996) are needed to generate kernel matrices of spheroids for larger x. These range limitations restrict the inversion computations to the particle size range of $0.05 \leq r \leq 7$ μm for λ from 0.44 to 1.02 μm.

In this work, we have applied this inversion methodology during Saharan dust intrusions over Granada (far from Saharan dust sources). Therefore, dust particles with very large size are not expected to reach the area of study due to the deposition processes during the long path way travelled by these particles.

On the other hand, Mishchenko et al. (1997) showed that the simplest model with the same axis ratio distribution for spheroids of all sizes can adequately reproduce the phase functions measured for desert dust. This assumption is in agreement with other studies of Saharan dust (e.g. Reid et al., 2003), showing that shape factors and aspect ratios do not have pronounced size dependence. Also, Dubovik et al. (2002) found strongly pronounced artefacts in phase functions for axis ratios smaller than 1.6 and larger than 2.2. They found that using equally mixed prolate and oblate spheroids with axis ratios from 1.6 to 2.2 resulted in superior retrievals compared to those obtained using spheroids of any single shape or other tested mixtures of shapes. In the inversion approach of this work we have used only the kernel matrices computed using equally mixed prolate and oblate (equiprobable distribution) for axis ratios equal to 1.6.

Using these kernel matrices, equation (3) is iteratively inverted in order to derive the effective columnar aerosol properties (refractive index, volume size distribution, single scattering albedo, asymmetry parameter and phase function). Taking into account the possible experimental errors in scattering angles close to sun-position (e.g. pointing errors) and the differences between aureole/sky radiance data (instabilities) (e.g. Torres et al., 2012), in our method only $R(\Theta,\lambda)$ values for $\Theta \geq 6^o$ are used as input for inversion retrievals. On the other hand, for scattering angles lower than 40° the effects of non-sphericity in phase functions are minimal.

In each iteration step, using the refractive index as a fixed value, the algorithm computes the effective volume size distribution, $V(r)$, by inversion of $\tau_a(\lambda)$ and $\beta(\Theta,\lambda)$, and the computed distribution is used as input for the radiative transfer code in order to simulate $R'(\Theta,\lambda)$, which is compared with the experimental $R(\Theta,\lambda)$

to evaluate de root mean square difference $\in(R)$. The process is repeated until $\in(R)$ is less than a given threshold (absolute convergence criterion), $\in(R)<0.005$ for the final loop in this work, being 10 the maximum number of loops; otherwise the solution is rejected. We also force a relative convergence criterion on each loop and a give-up minimum convergence criterion after 2nd-loop (0.2). Finally, the optimal aerosol parameters are retrieved by iteration varying the complex refractive index. The algorithm retrieves first the real part of the refractive index - assuming the imaginary part as zero- and then, fixing the real part, the imaginary part is retrieved. The retrievals are found minimizing the residuals between measured and simulated normalized sky radiances (<10%), and also minimizing the RMSE –root mean square error- between the measured and simulated aerosol optical depth values (RMSE<5%). The equation of the residuals applied to the sky radiances is:

$$\Delta = \sqrt{\frac{\sum_{\lambda,\Theta}\left[(R(\Theta,\lambda) - R'(\Theta,\lambda))/R(\Theta,\lambda)\right]}{N_\lambda N_\Theta}} \qquad (8)$$

where N_λ and N_Θ are the number of wavelengths and scattering angles measured.

An additional improvement introduced by the inversion method used in this study is the retrieval of aerosol single scattering albedo which was not retrieved by the original inversion method of Nakajima et al. (1996). The aerosol single scattering albedo can be estimated by:

$$SSA(\lambda) = \frac{\tau_{scat}(\lambda)}{\tau_{ext}(\lambda)} \qquad (9)$$

where $\tau_{scat}(\lambda)$ is derived by an equivalent integral to equation (7), substituting K_{ext} for K_{scat}, being K_{scat} the scattering kernel function.

Taking into account the refractive index values reported by different authors for diverse aerosol mixtures (e.g. D'Almeida et al., 1991), including dust particles, the real and imaginary refractive indices used in the iterative processes are varied in the ranges 1.33–1.60 (0.02 step) and 0–0.01 (0.0005 step) for the real part (n) and imaginary part (k), respectively. It is important to note that the refractive indices used in the iterative process are assumed invariant with wavelength. This assumption can introduce errors in effective columnar aerosol properties retrievals, since the entire weight of the spectral variation of aerosol parameters is associated to $R(\Theta)$ and $\tau_a(\lambda)$. On the other hand, the retrieval errors in n and k showed for different authors using the inversion algorithms are about 30-50% for n and 0.04 for k for high aerosol loading and solar zenith angle>50º (e.g. Dubovik et al., 2002b). Also, the authors show that the consideration of non-spherical scattering causes an artificial spectral dependence of n and only values derived for long wavelengths (870 and 1020 nm) are close to the true values. Using as input parameters in the inversion code the normalized sky radiance and the aerosol

optical depth, our experience shows that the assumption of a spectrally independent refractive index minimizes the instability on convergence criteria.

Accuracy assessment of individual retrievals

To analyze the accuracy of individual retrievals of the principal plane inversion method used in this work, an extensive sensitivity test was performed using computed data (simulations) and measurements characterized by different loads of mineral dust particles. The purpose of the numerical tests (simulations) is to verify the algorithm efficiency and check the results regarding the setting of the inversion algorithm.

We have conducted several numerical tests varying in coarse mode the particle mean radius, the volume concentrations, the standard deviations and the refractive index. In these test the properties of the fine mode are assumed as constant. Firstly, we retrieved the aerosol optical depths, the principal plane normalized sky radiances and the other aerosol parameters (direct method) using different dust-like aerosol models, varying the size distribution and refractive index, and using the non-spherical kernels computed in this work. The analysis was performed for 440, 670, 870 and 1020 nm wavelengths, and the maximum scattering angle used was 140°. Then, we applied the principal plane inversion algorithm to derive the aerosol optical parameters, using as input parameters the spectral aerosol optical depth and the normalized sky radiances retrieved by the direct method. The differences between retrieved and assumed values of aerosol properties give the apparent errors of the retrieval.

The following equation describes the bimodal log-normal model used in direct method:

$$\frac{dV(r)}{d\ln r} = \sum_{i=1}^{2} \frac{C_i}{\sqrt{2\pi}\sigma_i r} \exp\left[-\frac{(\ln r - \ln r_i)^2}{2\sigma_i^2} \right]$$

where $dV(r)/d\ln r$ is the particle volume size distribution, r is the particle radius, i denotes fine or coarse modes, C_i is the volume concentrations, and σ_i the standard deviations.

Table 1 shows an example of the parameters used in test to derive the aerosol properties by the direct method.

Table 1. Example of the aerosol parameters used in direct method.
(f: fine mode, c: coarse mode)

Volume mean radius	$r_{Vf} = 0.16$ $r_{Vc} = 1.33$
Ratio of particle concentration for volume distributions	$C_{Vf} / C_{Vc} = 0.05$
Standard deviations	$\sigma_f = 0.25$ $\sigma_c = 0.52$
Refractive Index	$n = 1.51$ $k = -0.002$

Given the importance of aerosol absorption to issues of radiative forcing, it is of interest to evaluate the agreement between values of single scattering albedo obtained for simulated (direct method) and inversion retrieved aerosol properties. Figure 2 shows the assessment for the effective single scattering albedo, volume size distribution, phase function and normalized sky radiances using simulated (from Table 1, direct method) and computed data (inversion method). As seen in Figure 2, the retrieved aerosol properties by the inversion procedure were close to the simulations. The RMSE% (root mean square error) computed for the data sets (direct method vs. inverted) –Figure 2-, including all wavelengths and/or scattering angles for each data set, is close to 1% for single scattering albedo, close to 2% for phase functions and close to 3% for normalized sky radiances. For the volume size distribution the RMSE% are close to 3% in coarse mode, but could increase up to 30% for radius close to 0.1 and 7 µm. Outside this range of radius the RMSE% increased drastically.

Figure 3 shows the relative deviations distribution of the retrieved $R(\Theta,\lambda)$ for the analyzed case (Table 1), that is computed as follows:

$$\frac{(R_{computed}(\Theta,\lambda) - R_{simulated}(\Theta,\lambda))}{R_{simulated}(\Theta,\lambda)}$$

As seen in Figure 3, the relative deviations have a clear angular dependence that increases for lower scattering angles and reaches a maximum of 12% at scattering angles close to 6º.

Similar results are obtained for the different dust-like aerosol models tested using the spheroid model. In all cases the optical parameters retrievals were performed with RMSE% close to 5% or less, and close to 10% or less for normalized sky radiances and volume size distributions. These results are in agreement with the criteria used in inversion algorithm for the cloud-screening method and also with the minimization of the normalized sky radiance residuals in the iterative procedure.

On the other hand, to analyze the behaviour of the inversion code taking into account the possible errors on input parameters (e.g. calibration or systematic errors) we have performed different test on experimental/simulations data with errors of 3% and 5% in $\tau_a(\lambda)$, $R(\Theta,\lambda)$ (also 7%), surface albedo and refractive index. These error variations also include the possible errors in radiance calibrations (e.g. Torres, 2012). As example, Figure 4 shows different results using experimental data corresponding to the Saharan dust event that affected Granada in June, 23 2008: a) effective size distributions derived using as input parameter $\tau_a(\lambda)\pm5\%$, b) $R(\Theta,\lambda)$ derived using as input parameter $\tau_a(\lambda)\pm5\%$, c) effective $SSA(\lambda)$ derived using as input parameter $R(\Theta,\lambda)$ and $R(\Theta,\lambda)+7\%$, and d) effective $SSA(\lambda)$ derived using as input parameter $\tau_a(\lambda)\pm5\%$. These results show that the computed RMSE% for the data sets of Figure 4 is less than 5% in all cases. Also, the different test performed show that the RMSE% from the retrieved optical parameters, in absence of strong systematic biases, was about 5% or less in all cases. Therefore, this residual value can be adopted as an indicator of the quality of the retrievals. In addition, Figure 5 shows the effective $SSA(\lambda)$ derived for this event at Granada using a spectrally constant value for the surface albedo (0.15) or using the spectrally dependence derived by AERONET network. The results show, in agreement with other authors (e.g. Dubovik et al., 2000, 2002b), that the $SSA(\lambda)$ is minimally affected by surface reflectance.

Finally, using this methodology and in view of the previous results, the accuracy of single scattering albedo and asymmetry parameters retrievals, for mineral aerosol loading and the use of scattering angles up to 100º or greater, are about 5%. For volume size distributions the error depends on the particle size. For the interval $0.1\leq r \leq 7$ μm the retrieval errors do not exceed 10%. Even taking into account the limitations of this methodology, these results are comparable to those derived by other authors using the almucantar configuration (e.g. Dubovik et al., 2000; Dubovik et al., 2002b).

Comparison with the aerosol properties provided by AERONET.

In this section, first we compared the aerosol optical depths computed by our methodology and those provided by AERONET (level 2.0). The extinction measurements used are registered during the desert dust events detected over Granada from 2005 to 2010. It is important to note that for computing AOD values by our method we used the pre- and post- calibration constants provided by AERONET, and also the same K7 raw files provided by the sun-photometer.

As example, Figure 6a shows the scatter plot of $AOD(670nm)$ data (level 2.0) provided by AERONET versus the computed by our methodology, including the cloud-screening method. As can be seen the AOD data obtained by both method are well correlated with correlation coefficient (R^2) of 0.99. The slope of linear fit is equal to 1 and the intercept value is very small (0.006). The mean absolute difference between the $AOD(670nm)$ computed by our method and the provided by AERONET is equal to 0.009. For $AOD(\lambda)$ at 440, 870 and 1020 nm the absolute differences are 0.009, 0.005 and 0.009, respectively (Table 2). Taking into account

the uncertainty in $AOD(\lambda)$ computations, these results show that there is an agreement between the $AOD(\lambda)$ computed by both methods.

Table 2 shows the comparison between $SSA(\lambda)$ and $g(\lambda)$ values retrieved by the principal plane inversion method and the AERONET almucantar inversion method at Granada during the desert dust events from 2005 to 2010. In this assessment only nearly coincident measurements are used. This assessment will be only relative since the different measurement time protocol for almucantar and principal plane sky radiances. On the other hand, there were few $SSA(\lambda)$ retrievals (level 2.0) at Granada due to the limitations imposed by the AERONET inversion algorithm (AOD (440 nm) > 0.4 and solar zenith angle > 50º). In this sense, we used for assessment $SSA(\lambda)$ values corresponding to the AERONET level 1.5 (cloud screened data that have pre- and post-calibrations applied). Furthermore, only $SSA(\lambda)$ retrievals for AOD (440 nm) > 0.2 and solar zenith angle > 50º are compared. Table 2 shows that the mean values of $SSA(\lambda)$ at 670, 870 and 1020 nm retrieved by the principal plane inversion algorithm are about 0.02 lower than those retrieved by AERONET inversion code. However, the single scattering albedo mean value at 440 nm computed by the principal plane inversion is 0.01 larger than the provided by AERONET code. These differences are within of the estimated error (0.03-0.07) for $SSA(\lambda)$. The root mean square error for $SSA(\lambda)$ ranges between 0.026 and 0.048 at 1020 and 440 nm, respectively. Figures 6b and 6c show the absolute differences of $SSA(670\ nm)$ and $g(670\ nm)$ computed by our methodology and AERONET method. As can be seen, up to 70% of the absolute differences are within the estimated error (0.02) for $g(\lambda)$. The root mean square error for $g(\lambda)$ varies between 0.031 and 0.043 at 440 and 1020 nm, respectively. In all channels the spectral asymmetry parameter mean values computed using our method are smaller than AERONET asymmetry parameters. The differences obtained between the two data sets could be due to the differences in measurement time and inversion algorithms.

Figure 7 shows an example of the temporal evolution of $SSA(440\ nm)$ and $g(440\ nm)$ computed by the two methodologies for June 23 (2008). The AERONET data set are level 2.0 data. Taking into account the uncertainty in both optical parameters, Figure 7 shows that $SSA(440\ nm)$ and $g(440\ nm)$ obtained by the two methods are comparable. The mean daily values (± standard deviations) of $SSA(440\ nm)$ and $g(440\ nm)$ are 0.90±0.01 and 0.74±0.01 for the AERONET inversion code (almucantar configuration), and 0.89±0.02 and 0.71±0.01 for the principal plane code, respectively. The differences obtained are due to the different input parameters (almucantar and principal plane radiances), time measurements, different kernel matrices, and also to the internal restrictions and convergence levels of both codes. Moreover, in this case we do not observe the possible artefacts in the retrievals, due to the experimental pointing errors, such as those shown by Torres (2012): lower values of $SSA(\lambda)$ for smaller solar zenith angles. The differences for the asymmetry parameter in this day (Figure 7 b) correspond to higher solar zenith angles, and can be related to the different kernel matrices used. These results indicate that we need accurate modelling of the phase functions at scattering angles ≥90º. Similar results are obtained for other days affected by high load of Saharan dust particles at Granada (AERONET level 2.0 data).

Comparison with in situ measurements

Finally, it would be interesting to compare the size distributions derived from the principal plane inversion code with in situ techniques. Many groups and institutions have focused on this purpose using ground-based instruments, Lidar technologies, aircraft instrumented, satellite, etc in different experimental campaigns. They have found agreements but also some discrepancies (e.g. Molero et al., 2005; Müller et al., 2010a,b).

In this work we present a comparison of columnar versus ground-based measurements of aerosol volume size distribution in a case of long-range transport of desert dust. Measurements were taken during the field campaign VELETA-2002, carried out in Granada (Spain). In this campaign, a rather complete characterization of the atmospheric aerosol was obtained by simultaneously measuring the columnar aerosol characteristics, by means of CIMEL-C318 sun-photometers, the size-segregated near-surface aerosol mass concentration by a GRIMM 1108 dust monitor and aerosol vertical extinction coefficient profiles by a lidar system (e.g. Molero et al., 2005; Estellés et al., 2006; Alados-Arboledas et al., 2008). For this task, we have re-computed the columnar volume size distributions using the principal plane inversion algorithm, and taking into account the K7 raw files provided by the sun-photometer located at Armilla station (e.g. Alados-Arboledas et al., 2008).

As example, Figure 8 shows the columnar volume size distribution computed vs. the GRIMM measurements integrated to the column by means of the scale height provided by the lidar system. This Figure corresponds to measurements recorded on the morning of July 18, 2002. The fine mode was only partially measured by the GRIMM monitor due to the radius limitations of the instruments. In this day the measurements show that the boundary layer can not be considered as well-mixed because of the arrival of the dust-rich air mass, but the results are comparable taking into account the error associated with both procedures. In this case there is an agreement of both techniques in the modes (fine and coarse) of $dV(r)/d\ln r$, even though the comparison of the remote sensing and in situ measurements is rather difficult and uncertain. Also, the algorithm constrains for particles larger than 7 μm do not overestimated the fine mode size distribution taking into account the error related to the methodology.

Table 2. Mean values (±standard deviation) of spectral aerosol optical depth (*AOD*), single scattering albedo (*SSA*) and asymmetry parameter (*g*); RMSE is their root mean square error and Δ refers the absolute differences between retrievals obtained by our method and the AERONET code at 440, 670, 870 and 1020 nm for all nearly coincident measurements during desert dust events from 2005 to 2010. Subscript "*a*" and "*n*" refers to AERONET and our method, respectively.

	440 nm	670 nm	870nm	1020nm
$AOD_a(\lambda)$	0.27±0.15	0.22±0.15	0.21±0.14	0.20±0.13
$AOD_n(\lambda)$	0.28±0.15	0.23±0.14	0.21±0.14	0.20±0.13
$SSA_a(\lambda)$	0.89±0.03	0.93±0.02	0.94±0.02	0.95±0.02
$SSA_n(\lambda)$	0.90±0.03	0.91±0.03	0.92±0.03	0.93±0.03
$g_a(\lambda)$	0.72±0.02	0.70±0.02	0.70±0.02	0.71±0.02
$g_n(\lambda)$	0.70±0.02	0.67±0.02	0.66±0.02	0.67±0.02
RMSE (*AOD(λ)*)	0.007	0.012	0.007	0.012
RMSE (*SSA(λ)*)	0.048	0.034	0.028	0.026
RMSE (*g(λ)*)	0.031	0.036	0.042	0.043
$\Delta AOD(\lambda)$	0.009±0.008	0.009±0.009	0.005±0.006	0.009±0.008
$\Delta SSA(\lambda)$	0.037±0.031	0.027±0.021	0.022±0.018	0.021±0.016
$\Delta g(\lambda)$	0.026±0.017	0.033±0.014	0.039±0.015	0.039±0.016

Figure 1. a) All-sky image registered for October 6, 2010, 10:15 h GMT –cloudless-; b) for October 7, 2010, 10:15 h GMT –clouds-; and c) normalized principal plane sky radiances derived for the two situations.
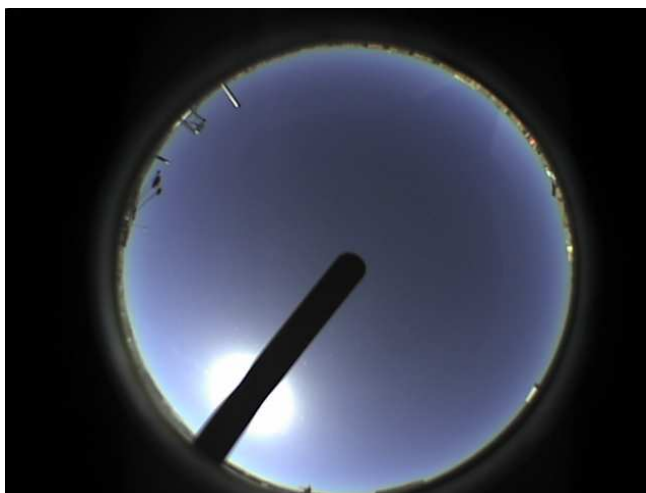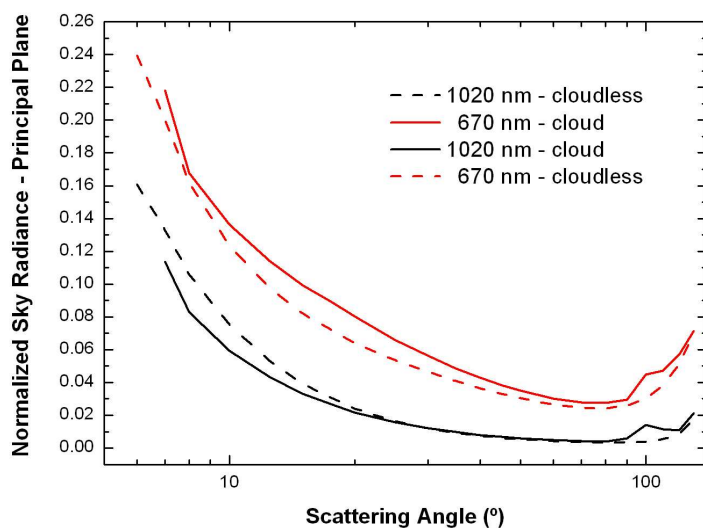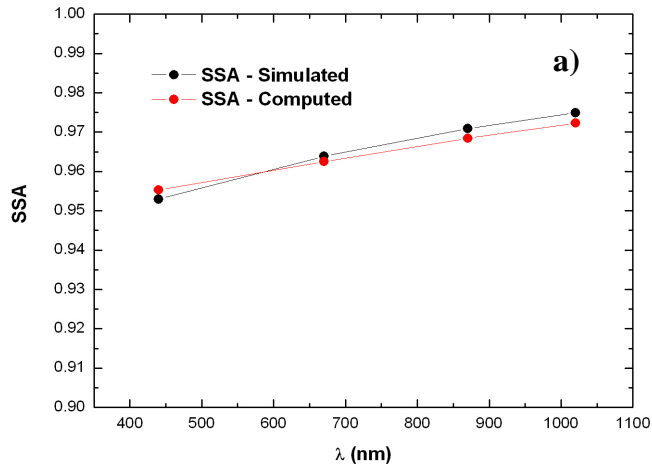
Figure 2. Evaluation of simulated (direct method) and retrieved (inversion) data: a) *SSA(λ)*, b) Volume size distribution, c) Phase function, and d) Normalized sky radiance in the principal plane.
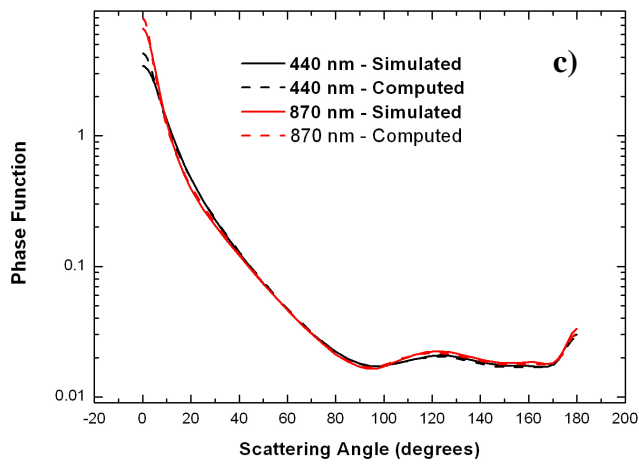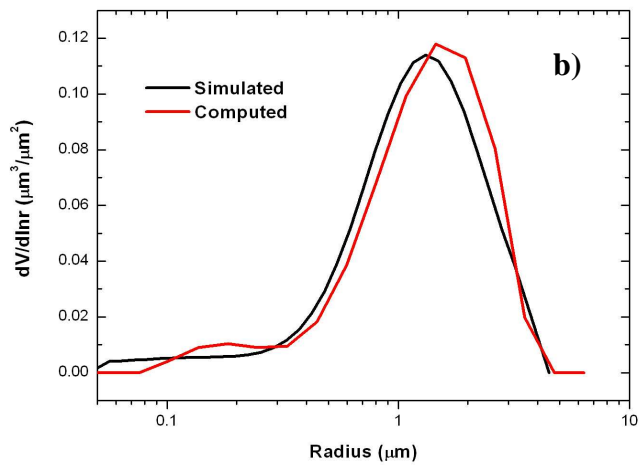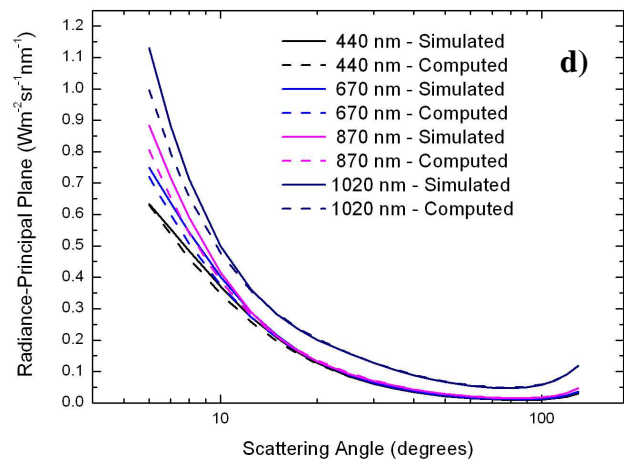
Figure 3. Relative deviations distribution of retrieved $R(\Theta,\lambda)$ by inversion vs. simulated data –direct method- (from Table 1).
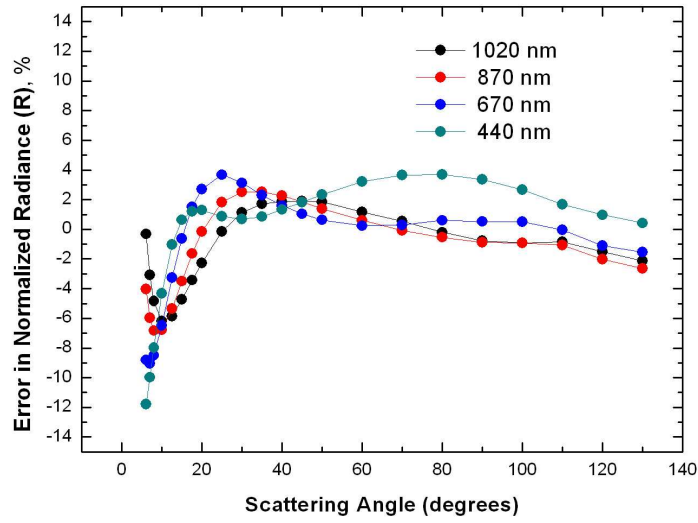
Figure 4. Results for different effective aerosol optical parameters using experimental data corresponding to the Saharan dust event detected over Granada in June, 23 2008: a) volume size distributions derived using as input parameter $\tau_a(\lambda)\pm5\%$, b) $R(\Theta,\lambda)$ derived using as input parameter $AOD(\lambda)\pm5\%$, c) SSA(λ) derived using as input parameter $R(\Theta,\lambda)$ and $R(\Theta,\lambda)+7\%$, d) $SSA(\lambda)$ derived using as input parameter $\tau_a(\lambda)\pm5\%$.
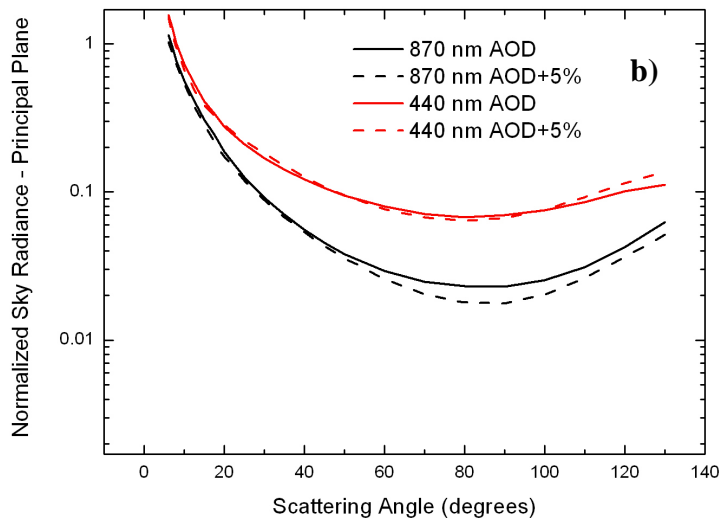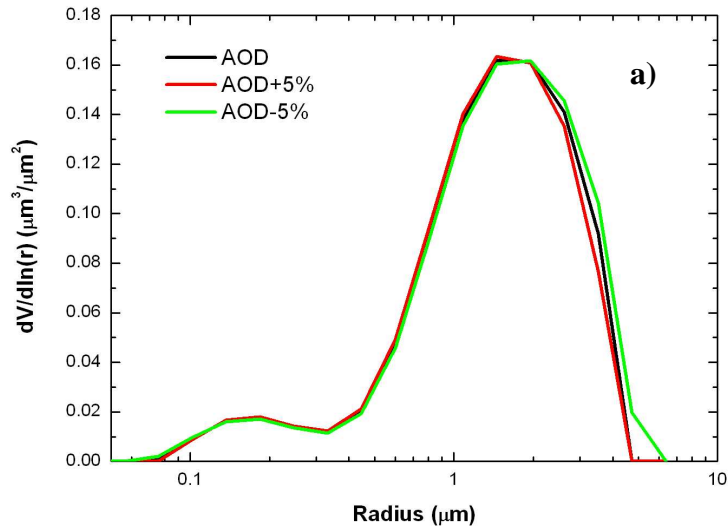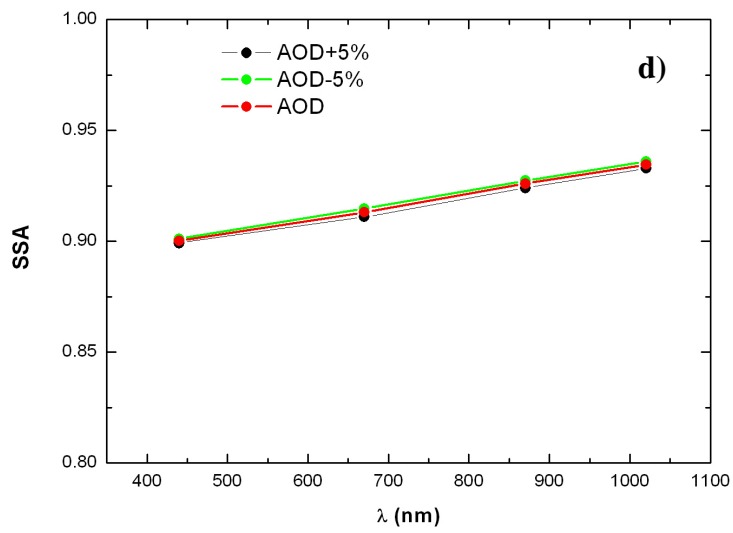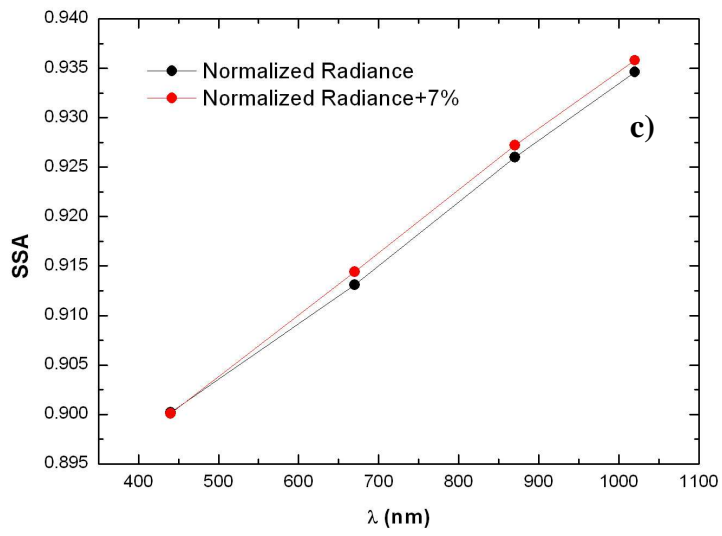
Figure 5. *SSA(λ)* derived using a spectrally constant value for the surface albedo (A) at Granada (June 23, 2008) and using the spectrally dependence of A derived by AERONET network.
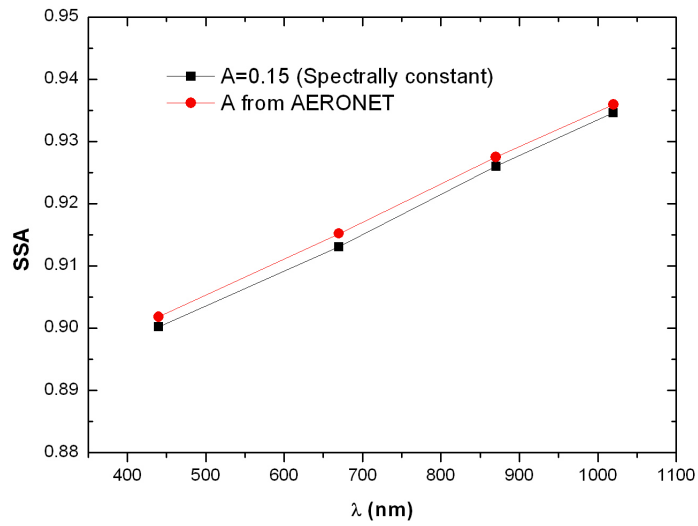
Figure 6. a) $AOD(670nm)$, b) absolute differences of $SSA(670nm)$ and c) absolute differences of $g(670nm)$ of level 2 provided by AERONET vs. the computed by our methodology.
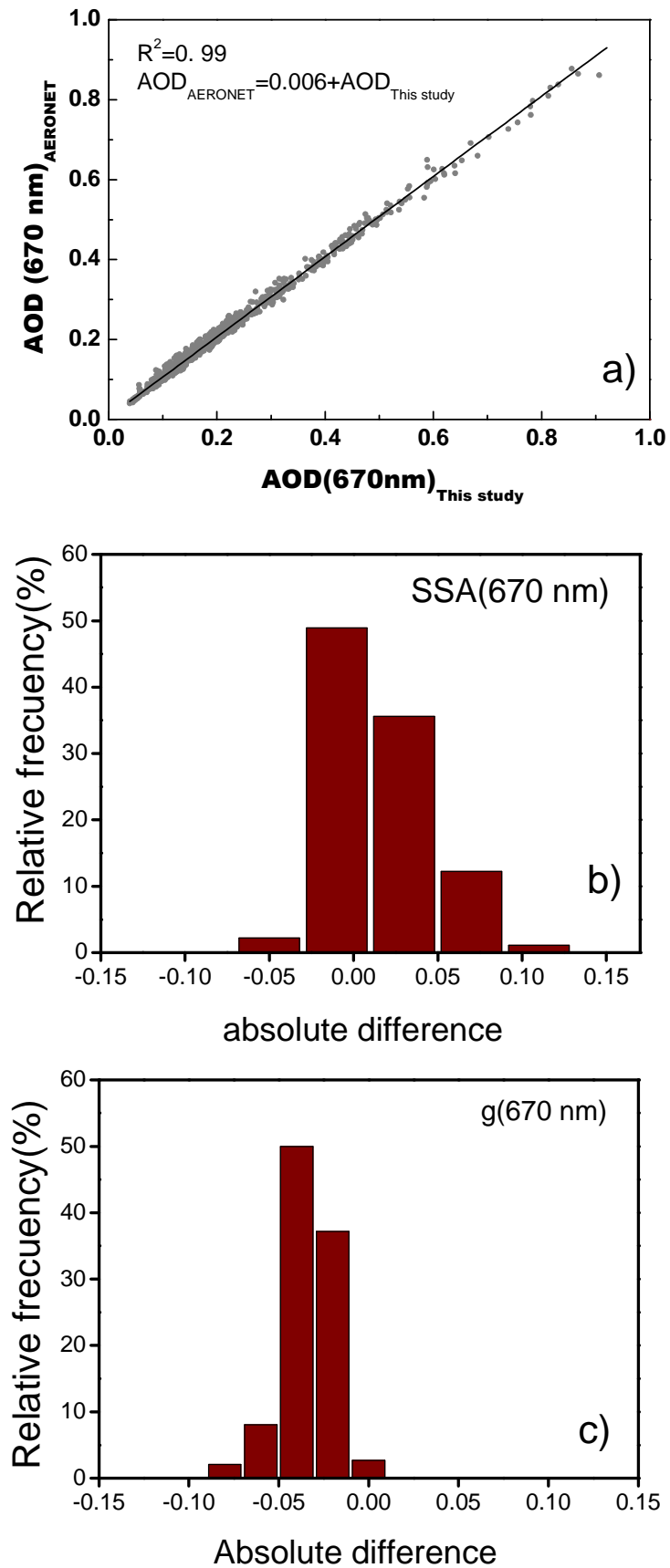
Figure 7. a) *SSA*(440*nm*) and b) g(440 nm) evolutions derived by AERONET code (Level 2.0 data) and by the Principal plane inversion code at Granada (June 23, 2008).
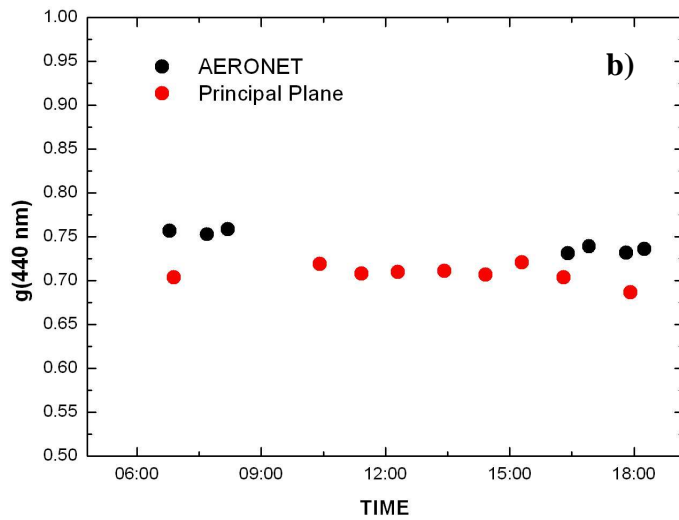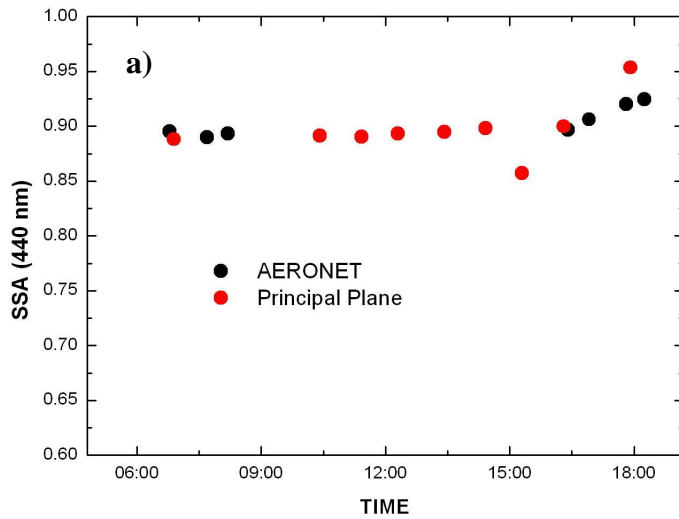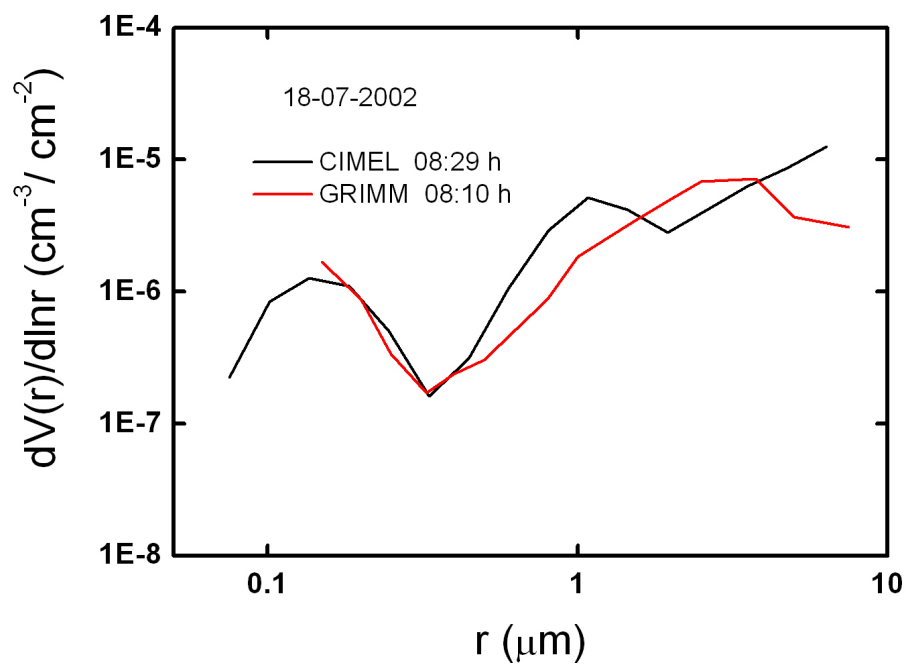
Figure 8. Columnar volume size distribution computed vs. the GRIMM measurements integrated to the column by means of the scale height provided by the lidar system (18th July, 2002).

REFERENCES:

Alados-Arboledas, L., Lyamani, H., Olmo, F.J.: Aerosol size properties at Armilla, Granada (Spain), Q. J. R. Meteorol.Soc., 129, 1395-1413, 2003.

Alados-Arboledas, L., A. Alcántara, F.J. Olmo, J.A. Martínez-Lozano, V. Estellés, V. Cachorro, A.M. Silva, H. Horvath, M. Gangl, A. Díaz, M. Pujadas, J. Lorente, A. Labajo, M. Sorribas, and G. Pavese.: Aerosol columnar properties retrieved from CIMEL radiometers during VELETA 2002, Atmos. Environ., 42, 2654–2667, 2008.

Bush, B.C., and Valero, F.P.J.: Surface aerosol radiative forcing at Gosan during the ACE-Asia campaign, J. Geophys. Res., 108, D23, 8660, doi:10.1029/2002JD003233, 2003.

Cazorla, A., Olmo, F.J., Alados-Arboledas, L.: Development of a sky imager for cloud covers assessment. Journal Optical Society of America – A, 25 (1), 29-38, 2008.

Dubovik, O., and King M. D.: A flexible inversion algorithm for retrieval of aerosol optical properties from sun and sky radiance measurements, J. Geophys. Res., 105, 20,673–20,696, 2000.

Dubovik O, Holben BN, Lapyonok T, Sinyuk A, Mishchenko M.I., Yang P, and Slutsker, I. : Non-spherical aerosol retrieval method employing light scattering by spheroids, Geophys. Res. Lett., 29(N10), 1415, doi:10.1029/2001GL014506, 2002a.

Dubovik, O., Holben, B., Eck, T.F., Smirnov, A., Kaufman, Y.J., King, M.D., Tanre, D., Slutsker, I.: Variability of absorption and optical properties of key aerosol types observed in worldwide locations, J. Atmos. Sci., 59, 590-608, 2002b.

Dubovik, O., Sinyuk, A., Lapyonok, T., Holben, B.N., Mishchenko, M., Yang, P., Eck, T.F., Volten, H., Muñoz, O., Veihelmann, B., van der Zande, W.J., Leon, J.F., Sorokin, M., Slutsker, I.: Application of spheroid models to account for aerosol particle nonsphericity in remote sensing of desert dust, J. Geophys. Res., 111, D11208, doi:10.1029/2005JD006619, 2006.

Estellés, V., Utrillas, M. P., Martínez-Lozano, J. A., Alcántara, A., Alados-Arboledas, L., Olmo, F. J., Lorente, J., de Cabo, X., Cachorro, V., Horvath, H., Labajo, A., Sorribas, M., Díaz, J. P., Díaz, A. M., Silva, A. M., Elías, T., Pujadas, M., Rodrigues, J. A., Cañada, J., García, Y.: Intercomparison of spectroradiometers and Sun photometers for the determination of the aerosol optical depth during the VELETA-2002 field campaign, J. Geophys. Res., 111, D17207, doi:10.1029/2005JD006047, 2006.

Holben, B.N., Eck, T.F., Slutsker, I., Smirnov, A., Sinyuk, A., Schafer, J., Giles, D., Dubovik, O. (2006). AERONET's Version 2.0 quality assurance criteria – art. nº

64080Q. In Remote Sensing of the Atmosphere and Clouds (edited by Tsay, S.C., Nakajima, T., Singh, R.P. and Sridharan, R.), vol. 6408 of PROCEEDINGS OF THE SOCIETY OF PHOTO-OPTICAL INSTRUMENTATION ENGINEERS (SPIE), p. Q4080.2006. ISBN 978-0-8194-6515-3, ISSN 0277-786X. Conference on Remote Sensing of the Atmosphere and Clouds, Goa, India, Nov. 13-16, 2006.

Kim, D.H., Sohn, B.J., Nakajima, T., Takamura, T., Takemura, T., Choi, B.C., Yoon, S.C.: Aerosol optical properties over east Asia determined from ground-based sky radiation measurements, J. Geophys. Res., 109, D02209, 18, doi:10.1029/2003JD003387, 2004.

Kobayashi, E., Uchiyama, A., Yamakazi, A., Kudo, R.: Retrieval of aerosol optical properties based on the spheroid model, Journal of the Meteorological Society of Japan, 88(5), 847-856, 2010.

Kokhanovsky, A.A., Budak, V.P., Cornet, C., Duan, M., Emde, C., Katsev, I.L., Klyukov, D.A., Korkin, S.V., C-Labonnote, L., Mayer, B., Min, Q., Nakajima, T., Ota, Y., Prikhach, A.S., Rozanov, V., Yokota, T., Zege, E.P.: Benchmark results in vector atmospheric radiative transfer, J. Quant. Spectrosc. Radiat. Transfer., 111 (12-13), 1931-1946, 2010.

Liou, K.N.: An introduction to Atmospheric Radiation. Elsevier, New York, 583 pp.

Lucht, W., and Roujean, J. L.: Consideration in parametric modeling of BRDF and albedo from multi-angular satellite sensors observations, Remote Sens. Rev., 18, 343– 379, 2000.

Mishchenko MI.: Light scattering by size-shape distributions of randomly oriented axially symmetric particles of a size comparable to a wavelength, Appl. Opt., 32, 4652–4666, 1993.

Mishchenko MI, Travis LD, Kahn RA, West RA.: Modeling phase functions for dust like tropospheric aerosols using a shape mixture of randomly oriented polydisperse spheroids, J. Geophys. Res., 102(D14), 16831–16848, 1997.

Molero, F., Alados-Arboledas, L., Pujadas, M., Antonio Alcantara, A., Victoria Cachorro, V., Estellés, V., Olmo, F. J., Martínez-Lozano, J. A., Lorente, J., Diaz, J. P., Labajo, A., De La Morena, B., Horvath, H. and Silva, A. M.: Comparison of aerosol size distributions measured at ground level and calculated from inversion of solar radiances, in Remote Sensing of Clouds and the Atmosphere, edited by K. Schafer et al., Proc. SPIE, 5979, 59790O, doi:10.1117/12.626993, 2005.

Moody, E.G., King, M. D., Platnick, S., Schaaf C.B., Gao F.: Spatially complete global spectral surface albedos: value-added datasets derived from Terra MODIS land products, IEEE Transactions on Geoscience and Remote Sensing, 43, 144-158, 2005.

Müller, D., Weinzierl, B., Petzold, A., Kandler, K., Ansmann, A., Mueller, T., Tesche, M., Freudenthaler, V., Esselborn, M., Heese, B., Althausen, D., Schladitz, A., Otto, S., Knippertz, P.: Mineral dust observed with AERONET Sun photometer, Raman lidar, and in situ instruments during SAMUM 2006: Shape-independent particle properties, Journal of Geophysical Research-Atmospheres 115, D11207, doi:10.1029/2009JD012523, 2010a.

Müller, D., Ansmann, A., Freudenthaler, V., Kandler, K., Toledano, C., Hiebsch, A., Gasteiger, J., Esselborn, M., Tesche, M., Heese, B., Althausen, D., Weinzierl, B., Petzold, A. and von Hoyningen-Huene, W.: Mineral dust observed with AERONET Sun photometer, Raman lidar, and in situ instruments during SAMUM 2006: Shape-dependent particle properties, Journal of Geophysical Research-Atmospheres 115, D11207, doi:10.1029/2009JD012523, 2010b.

Nakajima, T., Tonna, G., Rao, R.Z., Boi, P., Kaufman, Y., Holben, B.: Use of sky brightness measurements from ground for remote sensing of particulate polydispersions, Appl. Opt., 35, 2672-2686, 1996.

Phillips, D.: A technique for numerical solution of certain integral equations of first kind, Journal of the ACM, 9(1), 84-97, 1962.

Olmo, F.J., Quirantes, A., Alcantara, A., Lyamani, H., Alados-Arboledas, L.: Preliminary results of a non-spherical aerosol method for the retrieval of the atmospheric aerosol optical properties, J. Quant. Spectrosc. Radiat. Transfer., 100, 305-314, 2006.

Olmo, F.J., Quirantes, A., Lara, V., Lyamani, H., Alados-Arboledas, L.: Aerosol optical properties assessed by an inversion method using the solar principal plane for non-spherical particles, J. Quant. Spectrosc. Radiat. Transfer., 109, 1504-1516, 2008.

Reid, J.S., Jonsson, H.H., Maring, H.B., Smirnov, A., Savoie, D.L., Cliff, S.S., Reid, E.A., Livingston, J.M., Meier, M.M., Dubovik, O., Tsay, S.C.: Comparison of size and morphological measurements of coarse mode dust particles from Africa, J Geophys. Res., 108, D19, 8593, doi:10.1029/2002JD002485, 2003.

Smirnov, A., Holben, B.N., Eck, T.F., Dubovik, O., Slutsker, I.: Cloud-screening and quality control algorithms for the AERONET database, Remote Sens. Rev., 73, 337-349, 2000.

Stamnes, K. and Dale, H.: A new look at the discrete ordinate method for radiative-transfer calculations in anisotropically scattering atmospheres. II: intensity computations, J. Atmos. Sci., 38(12), 2696-2706, 1981.

Torres, B. (2012). Study on the influence of different error sources on sky radiance measurements and inversion-derived aerosol products in the frame of AERONET. Ph. D. Atmospheric Optics Group. University of Valladolid, April, 2012.

Waterman PC.:Symmetry, unitarity, and geometry in electromagnetic scattering, Phys. Rev, D3:825–839, 1971.

Wiscombe, W.: Delta-M Method – Rapid yet accurate radiative flux calculations for strongly asymmetric phase functions, J. Atmos. Sci., 34 (9), 1408-1422, 1977.

Yang, P., and K. N. Liou: Geometric-optics-integral-equation method for light scattering by nonspherical ice crystals, Appl. Opt., 35, 6568–6584, 1996.